University of Nebraska - Lincoln

DigitalCommons@University of Nebraska - Lincoln

Robert Powers Publications   Published Research - Department of Chemistry

1995

^{1}H, ^{15}N, ^{13}C and ^{13}CO Assignments and Secondary Structure Determination of Basic Fibroblast Growth Factor Using 3D Heteronuclear NMR Spectroscopy

Franklin J. Moy
Department of Structural Biology, Medical Research Division, Wyeth-Ayerst Research, Pearl River, NY

Andrew P. Seddon
Department of Protein Chemistry, Medical Research Division, Wyeth-Ayerst Research, Pearl River, NY

Ernest B. Campbell
Department of Protein Chemistry, Medical Research Division, Wyeth-Ayerst Research, Pearl River, NY

Peter Böhlen
Department of Protein Chemistry, Medical Research Division, Wyeth-Ayerst Research, Pearl River, NY

Robert Powers
University of Nebraska - Lincoln, rpowers3@unl.edu

Follow this and additional works at: http://digitalcommons.unl.edu/chemistrypowers

^{1}H, ^{15}N, ^{13}C and ^{13}CO Assignments and Secondary Structure Determination of Basic Fibroblast Growth Factor Using 3D Heteronuclear NMR Spectroscopy

Franklin J. Moy,[1] Andrew P. Seddon,[2] Ernest B. Campbell,[2] Peter Böhlen,[2]

and Robert Powers[1]

1. Department of Structural Biology, Medical Research Division, Wyeth-Ayerst Research, Pearl River, NY 10965, USA
2. Department of Protein Chemistry, Medical Research Division, Wyeth-Ayerst Research, Pearl River, NY 10965, USA

Corresponding author – Robert Powers, email rpowers3@unl.edu

Abstract

The assignments of the ^{1}H, ^{15}N, ^{13}CO, and ^{13}C resonances of recombinant human basic fibroblast growth factor (FGF-2), a protein comprising 154 residues and with a molecular mass of 17.2 kDa, is presented based on a series of three-dimensional triple-resonance heteronuclear NMR experiments. These studies employ uniformly labeled ^{15}N- and ^{15}N-/^{13}C-labeled FGF-2 with an isotope incorporation > 95% for the protein expressed in *E. coli*. The sequence-specific backbone assignments were based primarily on the interresidue correlation of C^α, C^β, and H^α to the backbone amide ^{1}H and ^{15}N of the next residue in the CBCA(CO)NH and HBHA(CO)NH experiments and the intraresidue correlation of C^α, C^β, and H^α to the backbone amide ^{1}H and ^{15}N in the CBCANH and HNHA experiments. In addition, C^α and C^β chemical shift assignments were used to determine amino acid types. Sequential assignments were verified from carbonyl correlations observed in the HNCO and

HCACO experiments and C^α correlations from the HNCA experiment. Aliphatic side-chain spin systems were assigned primarily from H(CCO)NH and C(CO)NH experiments that correlate all the aliphatic ^{1}H and ^{13}C resonances of a given residue with the amide resonance of the next residue. Additional side-chain assignments were made from HCCH-COSY and HCCH-TOCSY experiments. The secondary structure of FGF-2 is based on NOE data involving the NH, H^α, and H^β protons as well as $^3J_{H^N H^\alpha}$ coupling constants, amide exchange, and $^{13}C^\alpha$ and $^{13}C^\beta$ secondary chemical shifts. It is shown that FGF-2 consists of 11 well-defined antiparallel β-sheets (residues 30–34, 39–44, 48–53, 62–67, 71–76, 81–85, 91–94, 103–108, 113–118, 123–125, and 148–152) and a helix-like structure (residues 131–136), which are connected primarily by tight turns. This structure differs from the refined X-ray crystal structures of FGF-2, where residues 131–136 were defined as β-strand XI. The discovery of the helix-like region in the primary heparin-binding site (residues 128–138) instead of the β-strand conformation described in the X-ray structures may have important implications in understanding the nature of heparin–FGF-2 interactions. In addition, two distinct conformations exist in solution for the N-terminal residues 9–28. This is consistent with the X-ray structures of FGF-2, where the first 17–19 residues were ill defined.

Keywords: triple-resonance spectroscopy; multidimensional NMR; ^{1}H, ^{15}N, ^{13}C, and ^{13}CO assignments; basic fibroblast growth factor

Introduction

Basic fibroblast growth factor (FGF-2) is a 17.2-kDa protein, consisting of 154 residues, which exhibits angiogenic and a variety of growth and differentiation activities. Its pleiotrophic nature suggests possible roles in tumor growth and wound healing, and the protein is thus an attractive target for therapeutic drug development (Folkman and Klagsbrun, 1987; Baird and Bohlen, 1990; Basilico and Moscatelli, 1992). FGF-2 belongs to a nine-membered family that includes three oncogenes (FGF-3, FGF-4, and FGF-5), characterized by a high affinity toward heparin sulfate proteoglycans (HSPG) and a high, 30–55%, sequence identity (Miyamoto et al., 1993). The interaction of FGF-2 with HSPG is required for binding to its cell-surface tyrosine kinase receptor (FGFR) and essential for mediating internalization and intracellular targeting (Yayon et al., 1991; Roghani and Moscatelli, 1992; Reiland and Rapraeger, 1993). Calorimetric binding studies and molecular modeling suggest that FGF-2 induces dimerization of FGFR, initiating transmembrane signaling (Pantoliano et al., 1994). Residues Lys[128], Arg[129], Lys[134], and Lys[138]* have been identified as part of the heparin-binding domain of FGF-2 (Li et al., 1994; Thompson et al., 1994). Heparin has also been shown to protect FGF-2 from inactivation resulting from exposure to low pH, elevated temperature or proteases, and to restore bioactivity to inactive growth factor (Westall et al., 1983; Gospodarowicz and Cheng, 1986; Saksela et al., 1988; Sommer and Rifkin, 1989; Pineda-Lucena et al., 1994a).

In order to better understand the mode of action of FGF-2 and in particular its interaction with HSPG and its cell surface receptor, we initiated a structural program to determine the three-dimensional structure of FGF-2 in solution by NMR spectroscopy. Here, we report the nearly complete ^{1}H, ^{15}N, ^{13}CO, and ^{13}C assignments of the spectrum of FGF-2 from a series of 3D triple-resonance experiments. These assignments have led to the determination of the solution secondary structure for FGF-2, based on NOE data involving the NH,

H^α, and H^β protons as well as $^3J_{H^NH^\alpha}$ coupling constants, amide exchange, and $^{13}C^\alpha$ and $^{13}C^\beta$ secondary chemical shifts. Two crystal structures have been reported for FGF-2, where the protein is described as a β-sheet barrel of six antiparallel β-strands with a base of six additional β-strands (Zhu et al., 1983; Ago et al., 1991; Eriksson et al., 1991; Zhang et al., 1991). Comparison between the NMR secondary structure and the refined X-ray structure indicates clearly similar structures; however, some distinct differences exist, particularly at the heparin-binding site.

Materials and Methods

Production of recombinant ^{15}N- and ^{13}C-/^{15}N-labeled FGF-2
The 154-residue form of Glu^{3,5} Ser^{78,96} human recombinant FGF-2 was expressed in *E. coli* essentially as described before (Seddon et al., 1991), except that cultures were grown in M9 minimal media containing [^{15}N]ammonium chloride (1.25 g/l) and [^{13}C]glucose (2 g/l) as the sole nitrogen and carbon sources. Cells from a 1 liter culture were harvested by centrifugation, resuspended in 30 ml of 50 mM Tris-HCl, pH 7.5, containing 0.1 mM EDTA and 0.6 M NaCl and disrupted by sonication (6 × 30 s pulses). About 50% of the expressed protein was in a soluble form and was purified as follows. After centrifugation (10000 × g; 20 min), the supernatant solution was incubated with 25 ml of hydrated heparin sepharose (Pharmacia Biotech, Piscataway, NJ) at 4°C for 1 h under constant rotation. The resin was isolated by centrifugation and washed extensively with 10 mM Tris-HCl, pH 7.4, containing 0.6 M NaCl; bound protein was eluted with Tris buffer containing 2 M NaCl. The 2 M NaCl eluent was diluted 10-fold with 50 mM sodium phosphate buffer (pH 7.2) and loaded onto a Mono S column (HR 5/5; Pharmacia Biotech). Elution of bound material was monitored at 280 nm and was accomplished using a linear salt gradient (0.1–1.0 M NaCl in 60 min) at a flow rate of 1.0 ml/min.

Labeled FGF-2 was also obtained from the insoluble fraction. The pellet was resuspended in 10 mM Tris (pH 7.8) containing 8 M urea, 10 mM DTT (30 ml/pellet from 1 l of cells) and incubated at room temperature for 30 min. Insoluble material was removed by centrifugation (27000 × g; 20 min) and the supernatant solution was loaded onto an S-sepharose column (25 ml), equilibrated with l0 mM Tris (pH 7.4) containing 8 M urea, 50 mM NaCl and 1 mM DTT at pH 7.4. After extensive washing, bound protein was eluted with the same buffer containing 0.35 M NaCl. Elution was monitored at 280 nm and fractions containing FGF-2 were pooled and diluted to 20 µg/ml with elution buffer and dialyzed (6 kDa cutoff) overnight against 18 l of 10 mM Tris buffer (pH 7.6) containing 1 mM DTT and 0.6 M NaCl at 4°C. Insoluble protein was removed by centrifugation, and the supernatant solution was loaded onto a heparin sepharose column (25 ml), equilibrated with 50 mM Tris (pH 7.4) containing 0.6 M NaCl; the bound protein was eluted with buffer containing 2 M NaCl. The final purification step was accomplished by Mono S anion exchange chromatography as described above.

These procedures typically yielded 8 mg and 6 mg of FGF-2 per liter of bacterial culture from the soluble and insoluble fractions, respectively. FGF-2 prepared from the soluble or insoluble fractions were indistinguishable by electrospray mass spectrometry, reversed-

phase HPLC, and NMR spectroscopy. Analyses by N-terminal sequence analysis and electrospray mass spectrometry were consistent with the 154-residue form of FGF-2 and indicated essentially complete removal of the N-terminal methionyl residue (introduced for expression of the mature protein). Isotope enrichments were >95% by electrospray mass spectrometry. Stock solutions of ^{13}C-/^{15}N- and ^{15}N-labeled FGF-2 at 1 mg/ml were stored in 50 mM sodium phosphate buffer (pH 7.2) containing 0.5 M NaC1 at --45°C.

NMR sample preparation
NMR samples of ^{13}C-/^{15}N- and ^{15}N-labeled FGF-2 in 90% H_2O/10% D_2O were prepared by concentration and buffer exchange of FGF-2 stock solutions using Centricon microconcentrators (10 kDa molecular weight cutoff; Amicon, Beverly, Massachusetts). Protein was exchanged into a buffer containing 50 mM potassium phosphate, 2 mM NaN_3 and 10 mM deuterated DTT in 90% H_2O/10% D_2O at pH 5.5, until the NaCl concentration was about 10 mM. ^{13}C-/^{15}N-labeled FGF-2 in 100% D_2O was prepared similarly until the H_2O concentration was about 10 mM. Sample concentrations were 1 mM (approximately 17 mg/ml) as determined spectrophotometrically (absorbance 0.1% at 280 nm = 0.964 (Thompson et al., 1994)).

DTT was required for the stability of the NMR sample. When DTT was omitted, a precipitate was observed within three days; however, in the presence of 10 mM DTT no signs of precipitation were observed after three months. Although two free cysteines, Cys[34] and Cys[101], remain in the Glu[3,5] Ser[78,96]-FGF-2 mutant, precipitation of protein in the absence of DTT was not a result of interdisulfide bond formation. Analysis of the precipitate after dissolving in 8 M urea by reversed-phase HPLC showed no evidence of oligomer formation; the HPLC profile was indistinguishable from that of an unprecipitated FGF-2 sample (data not shown). The addition of DTT had minimal effect on the FGF-2 ^{15}N-^{1}H HSQC spectra, indicating that the presence of DTT does not significantly alter the structure of the protein.

NMR spectroscopy
All NMR spectra were recorded at 25°C on a Bruker AMX-600 spectrometer equipped with a triple-resonance gradient probe. Water suppression was achieved either by presaturation during the recycle delay or through application of gradients via the WATERGATE sequence and homo-spoil pulses (Bax and Pochapsky, 1992; Sklenář et al., 1993). Quadrature detection in the indirectly detected dimensions was obtained in all cases using the TPPI-States method (Marion et al., 1989a).

Spectra were processed using the NMRPipe software package (Delaglio et al., 1995) and analyzed with PIPP (Garrett et al., 1991) and PEAK-SORT, an in-house software package. When appropriate, data processing included a solvent filter, zero-padding of the data to a power of two, linear back prediction of one data point of indirectly acquired data to obtain zero phase corrections (ph0 and ph1), and linear prediction of additional points for the indirectly acquired dimensions to increase resolution. Linear prediction by means of the mirror-image technique was used only for constant-time experiments. In all cases, data was processed with a skewed sine-bell apodization function and zero-filling (one time) was used in all dimensions.

CBCA(CO)NH, CBCANH, C(CO)NH, HC(CO)NH, and HBHA(CO)NH experiments were collected as described previously (Grzesiek and Bax, 1992a, 1993; Grzesick et al., 1993). Spectral widths in the indirectly detected ^{15}N, ^{13}C, and ^{1}H dimensions were 27.00, 55.97, and 6.67 ppm, respectively, with the carrier positions at 117.5, 47.0, and 4.75 ppm, respectively. The spectral width in the acquisition dimension was 13.44 ppm, with the carrier at the water frequency of 4.75 ppm. The numbers of points acquired were 32 complex points in F1 (^{15}N), 52 complex points in F2 (^{13}C or ^{1}H) and 1024 real points in F3 (^{1}H).

HNCO and HCACO experiments were collected as described previously (Powers et al., 1991a; Grzesiek and Bax, 1992b). Spectral widths in the indirectly detected ^{15}N, ^{13}C, and ^{13}CO dimensions were 21.92, 15.06, and 12.00 ppm, respectively, with the carrier positions at 117.5, 54.0, and 175.0 ppm. The spectral width in the acquisition dimension was 13.44 ppm for HNCO and 8.42 ppm for HCACO, with the carrier at the water frequency of 4.75 ppm. The numbers of points acquired were 32 complex points in F1 (^{15}N), 15 complex points in F2 (^{13}C), and 1024 real points in F3 (^{1}H). For the HNCO and HCACO experiments, 64 and 96 complex points were collected in F2 (^{13}CO), respectively.

HNHA and HNCA experiments were collected as described previously (Kay et al., 1990; Vuister and Bax, 1993). The spectral widths in the indirectly detected ^{15}N, ^{13}C, and ^{1}H dimensions were 27.00, 31.86, and 9.50 ppm, respectively, with the carrier positions at 117.5, 54.0, and 4.75 ppm. The spectral width in the acquisition dimension was 13.44 ppm, with the carrier at the water frequency of 4.75 ppm. The numbers of points acquired were 32 and 48 complex points in F1 (^{15}N) for HNCA and HNHA, respectively, 48 complex points in F2 (^{1}H) for HNHA and 54 complex points in F2 (^{13}C) for HNCA, and 1024 real points in F3 (^{1}H) for both.

HCCH-COSY and HCCH-TOCSY experiments were collected as described previously (Bax et al., 1990; Ikura et al., 1991). Spectral widths in the indirectly detected ^{13}C and ^{1}H dimensions were 33.13 and 8.01 ppm, respectively, with the carrier at 43.0 and 3.0 ppm, respectively. The spectral width in the acquisition dimension was 8.01 ppm, with the carrier at 3.0 ppm.

The ^{15}N-edited NOESY-HMQC and ^{13}C-edited NOESY-HMQC experiments were collected as described previously, with 100 and 120 ms mixing times, respectively (Marion et al., 1989b,c). Spectral widths in the indirectly detected ^{15}N and ^{13}C dimensions were 27.0 and 20.70 ppm, respectively, with the carrier positions at 117.5 and 64.0 ppm, respectively. For the direct and indirect ^{1}H dimensions in the ^{15}N-edited NOESY experiment, the spectral width was 13.44 ppm with the carrier at the water frequency of 4.75 ppm. For the ^{13}C-edited NOESY experiment, the spectral width was 9.16 ppm with the carrier at 4.00 ppm. The numbers of points acquired were 32 complex points in F1 (^{15}N or ^{13}C), 128 complex points in F2 (^{1}H), and 1024 real points in F3 (^{1}H).

$^{3}J_{H^{N}H^{\alpha}}$ coupling constants were obtained from the relative intensity of H^{α} crosspeaks compared to the NH diagonal in the HNHA spectrum (Vuister and Bax, 1993). Coupling constants were measured with a scaling factor of 1.1 for relaxation. Slowly exchanging NH protons were identified by recording an HSQC spectrum two days after exchanging an FGF-2 sample from H_2O to D_2O.

Results and Discussion

Resonance assignments

In general, the spectra obtained for FGF-2 were of excellent quality, with relatively high signal-to-noise ratio and chemical shift dispersion for a 17.2-kDa protein. The standard approach for backbone resonance assignments by the triple-resonance methodology is to maximize sequential correlations in an attempt to eliminate potential assignment ambiguities and to substantiate these assignments from side-chain spin system assignments (Clore et al., 1991; Powers et al., 1992). This ensures a high confidence level in the accuracy of the assignments. For FGF-2, because of the high quality of the spectra, we were able to determine the resonance assignments from a minimal number of experiments and sequential correlations, in conjunction with residue typing based on the C^α and C^β chemical shifts (Grzesiek and Bax, 1993).

The sequential assignments of FGF-2 essentially followed the semiautomated protocol described previously (Powers et al., 1992; Friedrichs et al., 1994). The assignments were based primarily on the correlations observed in four triple-resonance experiments. Specifically, the $C^\alpha(i)$-$^{15}N(i + 1)$-NH$(i + 1)$ and $C^\beta(i)$-$^{15}N(i + 1)$-NH$(i + 1)$ correlations were established from the CBCA(CO)NH experiment. The $C^\alpha(i)$-$^{15}N(i)$-NH(i) and $C^\beta(i)$-$^{15}N(i)$-NH(i) correlations, in addition to the interresidue correlations observed in the CBCA(CO)NH experiment, were established from the CBCANH experiment. The $H^\alpha(i)$-$^{15}N(i + 1)$-NH$(i + 1)$ correlations were established from the HBHA(CO)NH experiment. $H^\beta(i)$-$^{15}N(i + 1)$-NH$(i + 1)$ correlations were also observed in the HBHA(CO)NH experiment, but this information was not used for establishing sequential connectivity. The NH(i)-$^{15}N(i)$-H$^\alpha(i)$ correlations were established from the HNHA experiment. For FGF-2, the $C^\beta(i)$-$^{15}N(i)$-NH(i) correlation was by far the weakest, with only 82% of the expected crosspeaks being present. For the remaining correlations ≥ 93% of the expected crosspeaks were present. Figure 1 shows strips from the 3D CBCA(CO)NH, CBCANH, HBHA(CO)NH, and HNHA spectra, taken parallel to the F1 axis, for the amides of residues Phe[103] through Glu[108]. The ^{1}H, ^{15}N, ^{13}C, and ^{13}CO sequential resonance assignments are listed in table S1 (supplementary material) and have been deposited in the BioMagRes Databank (Seavey et al., 1991).
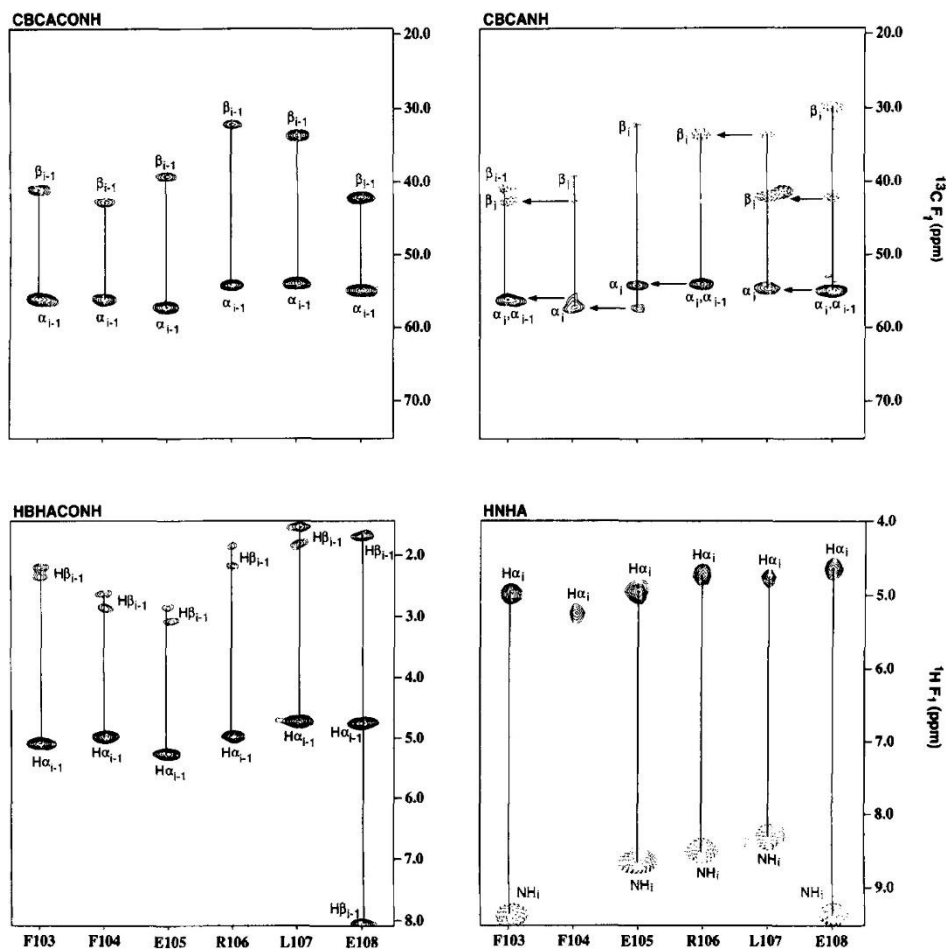
Figure 1. Strip plots taken from the CBCA(CO)NH, CBCANH, HBHA(CO)NH, and HNHA spectra for the amides of residues Phe[103] through Glu[108] of FGF-2. Each amide correlates with the C^α and C^β of the preceding residue (CBCA(CO)NH), with the H^α and H^β of the preceding residue (HNHA), and with its intraresidue C^α and C^β (CBCANH) and H^α atoms (HBHA(CO)NH). Intra- (i) and interresidue (i - 1) correlations are indicated with the observed interresidue connectivities marked by an arrow. Negative contours are indicated by dashed lines.

Even with the reasonably high number of observed crosspeaks, a significant number of sequential connections were initially based on only two or sometimes a single correlation. This was caused by the relatively high number of glycines (16) in the sequence and the relatively frequent occurrence (11) of identical $C^\alpha(i)$ and $C^\alpha(i-1)$ chemical shifts. Sequential assignments were also hindered by the presence of nine prolines, which caused breaks in the alignment due to the lack of an NH. These assignment problems were easily resolved using residue typing based on C^α and C^β chemical shifts, as proposed by Grzesiek and Bax (1993). This residue typing employs a probability distribution of the secondary C^α and C^β

chemical shifts, based on 600 chemical shifts collected from six different proteins. We collected C^α and C^β chemical shifts from an additional five proteins: IL-4, Che Y, profilin, dihydrofolate reductase, and RNase H (Carr et al., 1991; Powers et al., 1991b, 1992; Archer et al., 1993; Soteriou et al., 1993; Moy et al., 1994). Even with this expanded database, the data appeared to be better represented as a linear range of allowable chemical shifts, as opposed to a distribution of chemical shifts. Therefore, we made potential residue assignments based strictly on whether or not the observed pair of C^α and C^β chemical shifts fell within the allowed region for a particular residue type.

As a final step, the sequential assignments were verified by the $H^\alpha(i)$-$C^\alpha(i)$-CO(i) and NH(i)-^{15}N(i)-CO(i + 1) correlations observed in the HCACO and HNCO experiments, respectively, and to a lesser extent by the NH(i)-^{15}N(i)-$C^\alpha(i)$ and NH(i)-^{15}N(i)-$C^\alpha(i + 1)$ correlations observed in the HNCA experiment.

The ^{13}C and ^{1}H side-chain assignments were based primarily on the C^α, C^β, and H^α,H^β correlations observed from the CBCA(CO)NH and HBHA(CO)NH experiments, with the remainder of the side-chain information coming from the C(CO)NH and HC(CO)NH experiments, which correlate all the aliphatic ^{13}C or ^{1}H resonances of a given amino acid directly with the amide of the next residue. In this manner, 93% of the ^{13}C and 85% of the ^{1}H side-chain resonance assignments were made. Additional aliphatic ^{13}C or ^{1}H resonance assignments were obtained from the HCCH-COSY and HCCH-TOCSY experiments. Figure 2 shows strips from the C(CO)NH and HC(CO)NH spectra, taken parallel to the F1 axis, for the amides of residues Phe[103] through Glu[108]. The nearly complete side-chain aliphatic ^{13}C and ^{1}H resonance assignments are collected in table S1 (supplementary material). For completeness, the assignments of aromatic and amide side-chain resonances are also included. The aromatic side-chain assignments were obtained from intraresidue NOEs in the 3D ^{13}C-edited NOESY spectrum between the aromatic ring protons (C^δH of phenylalanine and tyrosine, $C^{\delta 2}$H of histidine, and $C^{\delta 1}$H and $C^{\delta 3}$H of tryptophan) and the H^α and H^β protons; the amide sidechain assignments of asparagine and glutamine were obtained from the interresidue NOEs between the NH_2 protons and the H^β and C^γH protons in the 3D ^{15}N-edited NOESY spectrum and verified in the CBCA(CO)NH experiment (data not shown).
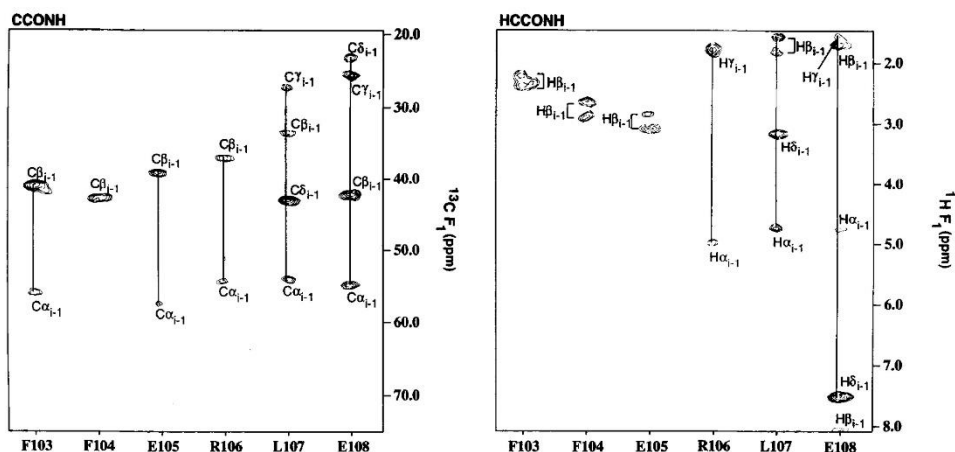
Figure 2. Strips taken from the C(CO)NH and HC(CO)NH spectra for the amides of residues Phe[103] through Glu[108]. Each amide correlates with the ^{13}C aliphatic (C(CO)NH) and proton (HC(CO)NH) resonances of the preceding residue's side chain. The solid line connects the correlations observed for each residue.

The use of the C(CO)NH experiment was crucial for obtaining the nearly complete side-chain assignments of FGF-2. The primary sequence of FGF-2 contains 25 arginine and lysine residues (~16% of the sequence), many of which are surface exposed, with ill-defined side-chain conformations. This results in near-degenerate aliphatic ^{13}C and ^1H resonances and severe overlap in the HCCH-COSY and HCCH-TOCSY spectra; however, the ^{15}N and NH chemical shift dispersion for FGF-2 was sufficiently large to allow for easy identification in the C(CO)NH spectra.

Secondary structure

The regular secondary structure elements of FGF-2 were identified from a qualitative analysis of sequential and interstrand NOEs, NH exchange rates, $^3J_{H^NH^\alpha}$ coupling constants and the $^{13}C^\alpha$ and $^{13}C^\beta$ secondary chemical shifts (Clore and Gronenborn, 1989; Spera and Bax, 1991). These data, together with the deduced secondary structure elements, are summarized in figure 3. The sequential and medium-range NOEs were obtained from a qualitative analysis of the ^{15}N-edited and ^{13}C-edited NOESY spectra, where box heights are related to peak intensity (fig. 4). $^3J_{H^NH^\alpha}$ coupling constants were measured for 111 of the 143 assigned non-proline residues and 53 of the 143 assigned non-proline amide protons were identified as very slow exchanging amide protons.
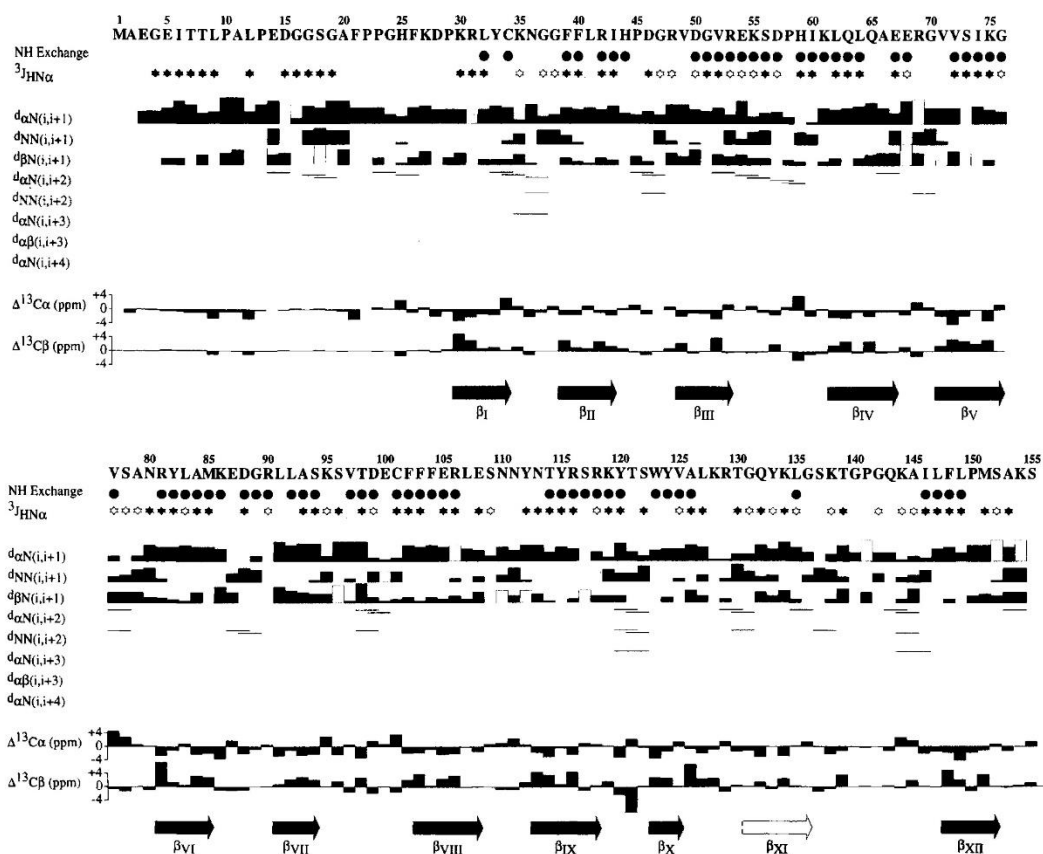
Figure 3. Summary of the sequential and medium-range NOEs involving the NH, Hα, and Hβ protons, the amide exchange and $^3J_{H^NH^\alpha}$ coupling constant data, and the $^{13}C^\alpha$ and $^{13}C^\beta$ secondary chemical shifts observed for FGF-2, with the secondary structure deduced from this data. The open arrow corresponds to strand XI observed in the FGF-2 X-ray structures. The thickness of the lines reflects the strength of the NOEs. Amide protons still present 48 h after exchange to D₂O are indicated by closed circles. The filled and open stars indicate $^3J_{H^NH^\alpha}$ values > 8 Hz and < 6 Hz, respectively. The open boxes represent potential sequential assignment NOEs that are obscured by resonance overlap and could therefore not be assigned unambiguously. The gray boxes on the same line as the Hα(i)-NH(i + 1) NOEs represent the sequential NOE between the Hα proton of residue i and the CδH proton of the i + 1 proline and are indicative of a trans proline.
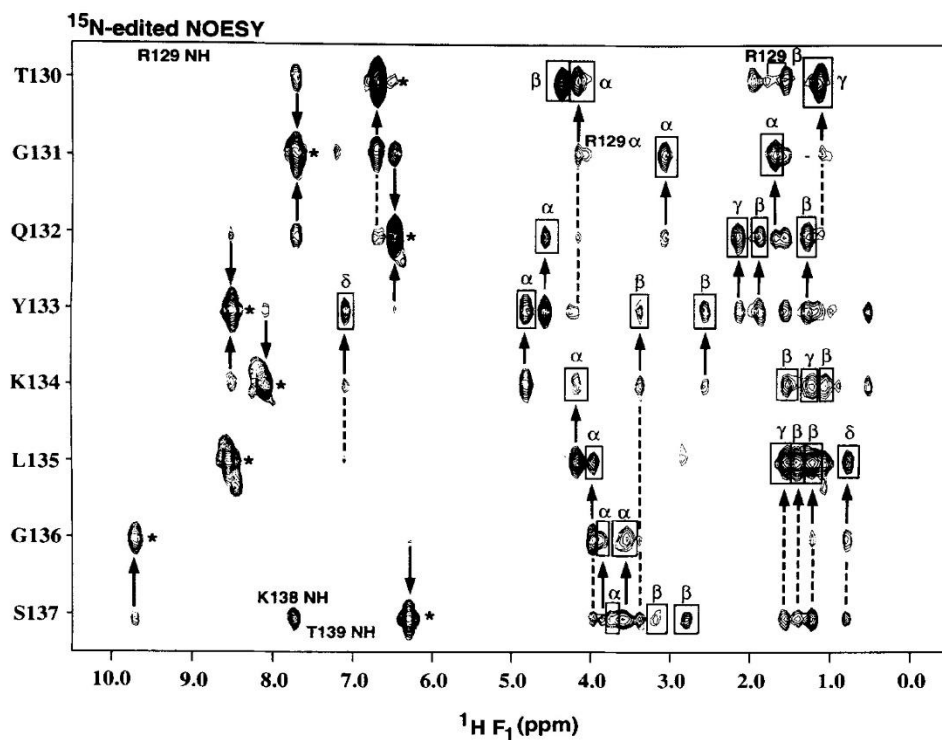
Figure 4. Composite of amide strips taken from the 3D ^{15}N-edited NOESY-HMQC spectrum (τ_m = 100 ms) of FGF-2 for the sequence stretch from Thr^{130} to Ser^{137}, corresponding to missing β-strand XI in the NMR structure. The diagonal peaks are indicated by an asterisk, NH(i)-NH(i ± 1), NH(i + 1)-H$^\alpha$(i), and NH(i)-NH(i ± 1) and NH(i + 1)-H$^\beta$(i) NOEs are indicated by solid arrows, and NH(i)-NH(i ± 2), NH(i + 2,3,4)-H$^\alpha$(i), and NH(i + 2,3,4)-H$^\beta$(i) NOEs are indicated by dashed arrows. Intraresidue H$^\alpha$-NH and H$^\beta$-NH NOEs are boxed.

It is apparent from the data in figure 3 that the FGF-2 structure is composed of a series of β-strands and turns. Interstrand H$^\alpha$ and NH NOEs observed in the ^{15}N-edited and ^{13}C-edited NOESY experiments clearly indicate the presence of three distinct antiparallel β-sheets, composed of 11 β-strands. This is further substantiated by observed stretches of strong sequential H$^\alpha$(i)-NH(i + 1) NOEs, weak or missing NH(i)-NH(i + 1) NOEs and missing medium-range (1 < |i − j| ≤ 4) NOEs, in combination with strong $^3J_{H^N H^\alpha}$ coupling constants and slowly exchanging amide protons. Using the β-strand numbering scheme from the X-ray structures, strand I extends from residue 30 to 34, strand II from 39 to 44, strand III from 48 to 53, strand IV from 62 to 67, strand V from 71 to 76, strand VI from 81 to 85, strand VII from 91 to 94, strand VIII from 103 to 108, strand IX from 113 to 118, strand X from 123 to 125, and strand XII from 148 to 152. The alignments of the three β-sheets are shown in figure 5. Turn conformations connecting various β-strands in the three antiparallel β-sheets are also clearly evident by the appearance of NH(i)-NH(i + 1) and medium-range, H$^\alpha$(i)-NH(i + 2,3) and NH(i)-NH(i + 2), NOEs in addition to weak $^3J_{H^N H^\alpha}$ coupling constants.
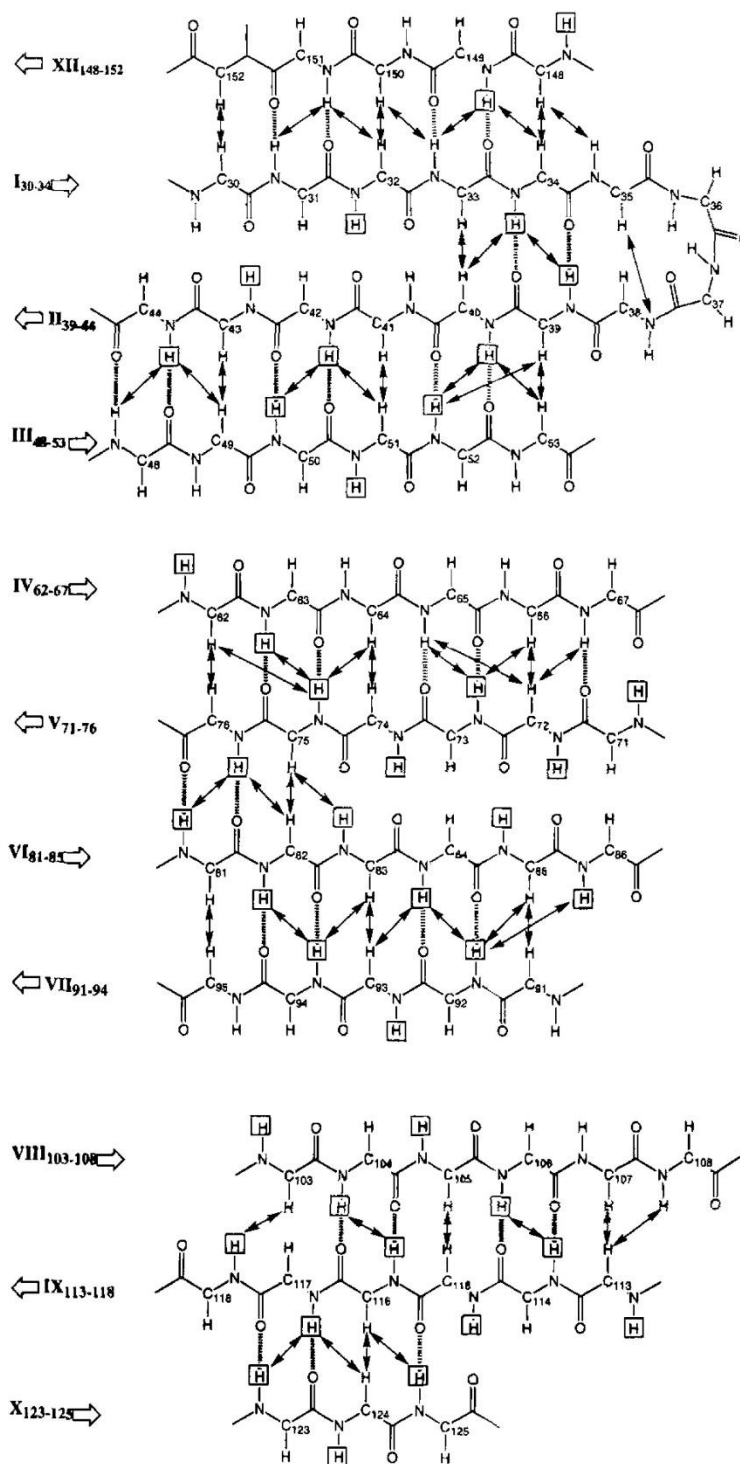
Figure 5. Secondary structure elements of FGF-2 as determined from qualitative analysis of the NOE and amide exchange data. The β-strands are indicated on the left by roman

numerals and the residue number range. Interstrand NOEs derived from the 3D ^{15}N- and ^{13}C-edited NOESY spectra are indicated by arrows, and slowly exchanging amide protons are boxed. The hydrogen bonds deduced from this data are shown as broken lines.

In general, the ^{13}C$^\alpha$ and ^{13}C$^\beta$ secondary chemical shifts are consistent with the identified regions of β-strands and turns, but it is obvious that there are regions that do not follow the expected trend (Spera and Bax, 1991). Thus, it was not possible to identify all the 13-strand regions based solely on the observed ^{13}C$^\alpha$ and ^{13}C$^\beta$ secondary chemical shifts. Comparison of the ^{13}C$^\alpha$ and ^{13}C$^\beta$ secondary chemical shifts for β-strands IV and V in figure 3 serves to illustrate this point. The ^{13}C$^\alpha$ and ^{13}C$^\beta$ secondary chemical shifts for strand V follow the expected trend, i.e., positive for ^{13}C$^\beta$ and negative for ^{13}C$^\alpha$. While strand IV contains residues that also follow this trend, a significant number of residues have ^{13}C$^\alpha$ and ^{13}C$^\beta$ secondary chemical shifts close to values for a random coil. Since the ^{13}C$^\alpha$ and ^{13}C$^\beta$ secondary chemical shifts are probably sensitive indicators of the local ϕ and ψ dihedral backbone angles, deviations from the expected trends are probably indicative of deviations from "ideal" β-strand conformation.

Comparison of the NMR and X-ray structure

The X-ray crystal structures show FGF-2 to be composed of 12 antiparallel β-strands, where six strands form a β-barrel and the remaining six form the base of a pyramid structure (Zhu et al., 1983; Ago et al., 1991; Eriksson et al., 1991; Zhang et al., 1991). The structures display a threefold repeat, corresponding to three groupings of four β-strands. The first 17–19 residues are not visible in the electron density map and have been identified as being disordered. The structure of FGF-2 has also been identified as a structural homolog of interleukin 1β (IL-1β), where a superposition of 96 residues comprising the β-cores of FGF-2 and IL-1β gave an rms deviation of 1.55 Å (Zhang et al., 1991). In general, the secondary structure elements identified from the NMR data are in good agreement with the X-ray data, including an explanation for the disorder observed for the first 17–19 residues.

The NMR data indicate that two distinct (major and minor) conformations exist in solution for the first 28 residues, as evident by two sets of sequential assignments for these residues. Based on the relative intensity of cross peaks in the ^{15}N HSQC spectra, it appears that the major and minor conformations exist at an approximate 3:1 ratio (fig. 6). The additional ^{1}H, ^{15}N, ^{13}C, and ^{13}CO sequential resonance assignments for the minor conformation are listed in table S2 (supplementary material). Since there are five prolines in the first 30 residues of FGF-2, it is reasonable to attribute the conformational differences to a cis-trans proline isomerization. The proline residues in the major FGF-2 conformation are all trans, as indicated by the H$^\alpha$(i)-C$^\delta$H(i + 1) NOEs in the ^{13}C-edited NOESY-HMQC spectrum. In the minor conformation, the prolines at positions 10 and 13 appear to have a cis conformation, as indicated by the low-field position of the C$^\beta$ resonance and the high-field position of the C$^\gamma$ resonance (Shirakawa et al., 1993). The presence of two distinct conformations in slow exchange would readily explain the weak electron density for the first 17–19 residues in the X-ray structure.
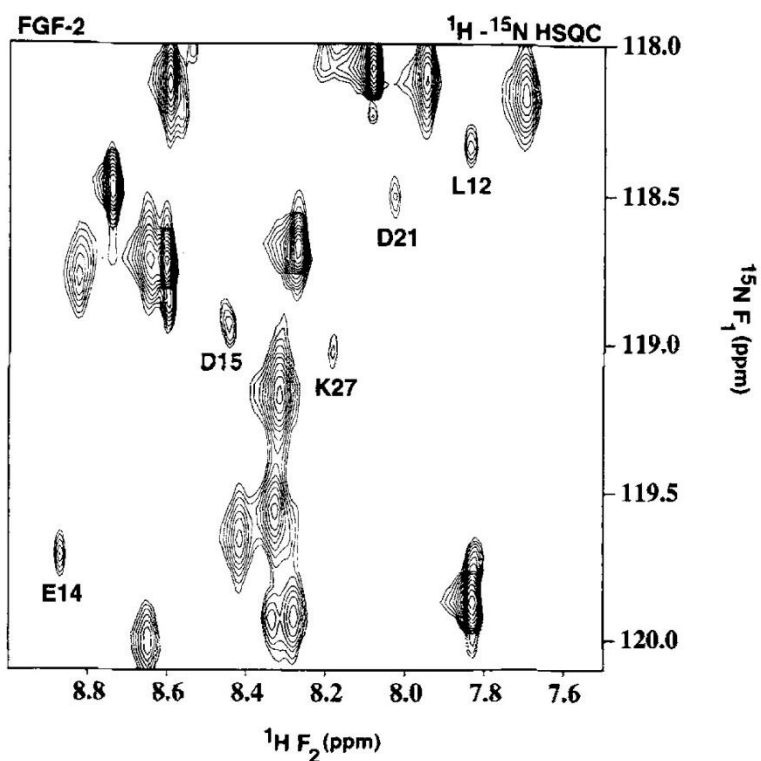
Figure 6. Expanded region of the ^{1}H-^{15}N HSQC spectrum. Peaks corresponding to the minor conformation of FGF-2 caused by the cis-trans isomerization of Pro[10] and Pro[13] are labeled.

The 11 antiparallel β-strands depicted in figure 5 align with the corresponding 13-strands in the X-ray structures, with only minor differences in the length of some of the strands. A direct comparison with the X-ray structure described by Eriksson et al. (1991) indicates that strand VII is one residue shorter, strands II, IV, and IX are longer by one residue, and strand XII is two residues longer in the NMR structure. In addition, strand X is shifted one residue toward the N-terminus in the NMR structure. It is also apparent that β-strand XI is not observed in the NMR structure. Figure 4 shows strips taken from the ^{15}N-edited NOESY spectrum, parallel to the F1 axis, for the amides of residues Thr[130] through Ser[137], which correspond to the residues described as β-strand XI in the X-ray structures. The NOE data presented are consistent with a turn or helix-like conformation, not with a β-strand conformation, as evidenced by the lack of interstrand H[α] and NH NOEs. The summary of structural data in figure 3 also supports this conclusion. Eriksson et al. (1991) noted that strand XI did not meet the criteria for β-sheet strands developed by Kabsch and Sander (1983), but that its location correlated with the β-strand framework from the IL-1β structures. It is important to note that the X-ray and NMR structures for IL-1β were very similar. In both structures, 12 β-strands were identified and a structure for IL-1β was refined from both the NMR and X-ray data (Clore and Gronenborn, 1991a,b).

An intriguing observation regarding the missing β-strand conformation for residues 131–136 in the NMR structure is the relative position of these residues with respect to the interaction of FGF-2 with HSPG. This interaction is essential for the binding of FGF-2 to its cell surface receptor and for its biologic activity (Yayon et al., 1991; Roghani and Moscatelli, 1992; Reiland and Rapraeger, 1993). Residues Lys[128], Arg[129], Lys[134], and Lys[138] have been identified as part of the heparin-binding domain of FGF-2 (Li et al., 1994; Thompson et al., 1994). These residues either correspond to or immediately flank the residues of β-strand XI defined in the X-ray structure, which appears to be more helix-like in the NMR structure. This might imply a structural role of heparin binding to FGF-2. It is reasonable to speculate that the binding of heparin to FGF-2 may induce proper formation of β-strand XI in solution and complete the third β-sheet formed by strands VIII to XI, and that this structural change is required for the binding of FGF-2 to its receptor. This is consistent with other observations, i.e., that the interaction of HSPG with a protein is determined by local structure instead of a consensus sequence (Seddon et al., 1991; Margalit et al., 1993; Li et al., 1994). From an analysis of defined heparin-binding sequences with known structures, Margalit et al. (1993) proposed a common heparin-binding motif of a β-strand or α-helix with two basic amino acids, separated by 20 Å.

The structural role of heparin binding to FGF-2 is also consistent with a known functional difference between IL-1β and FGF-2. IL-1β and FGF-2 are structural homologs, but IL-1β does not require heparin for activity. This suggests that FGF-2 requires heparin to stabilize β-strand XI, which is well formed in the IL-1β structure. This possibility is further substantiated by the NMR structure of acidic FGF (FGF-1) complexed with inositol hexasulfate (Pineda-Lucena et al., 1994b). The weakest interaction observed in the acidic FGF structure was the one between β-strands X and XI. The authors suggested that β-strands X and XI are stabilized by the interaction of inositol hexasulfate with the acidic FGF heparin-binding site, which is located at the end of β-strands X and XI.

Conclusions

Nearly complete ^{1}H, ^{15}N, ^{13}C, and ^{13}CO resonance assignments for human FGF-2 have been determined by three-dimensional triple-resonance heteronuclear NMR experiments. This is the first step toward determining a high-resolution NMR structure of FGF-2. The secondary structure elements present in FGF-2 have been identified based on a qualitative analysis of sequential and interstrand NOEs, NH exchange rates, ${}^3J_{H^NH^\alpha}$ coupling constants and the ${}^{13}C^\alpha$ and ${}^{13}C^\beta$ secondary chemical shifts. In general, the NMR structure agrees with the X-ray structures, including the observation that two distinct conformations in the NMR structure for the first 28 amino-terminal residues, caused by a cis-trans isomerization of Pro[10] and Pro[13], are consistent with the disorder observed for the first 17–19 residues in the X-ray structures. The major distinction between the NMR and X-ray structures is that β-strand XI in the X-ray structures appears more helix-like in the NMR structure. The helix-like conformation of residues 131–136 in the NMR structure suggests a possible structural role in the binding of heparin to FGF-2. Since residues 131–136 are in close proximity to the heparin binding site, and since heparin has been postulated to have a structure that is dependent on its binding, the interaction of heparin with FGF-2 could induce the proper

formation of β-strand XI, which might be required for receptor binding. The role of heparin in inducing an FGF-2 conformational change is under investigation.

Note

* The numbering for FGF-2 is from amino acid residue I, deduced from the cDNA sequence encoding the 155-residue form. The mature form comprises residues 2–155.

References

Ago, H., Kitagawa, Y., Fujishima, A., Matsuura, Y. and Katsube, Y. (1991) *J. Biochem.*, 110, 360–363.

Archer, S. J., Vinson, V. K., Pollard, T. D., and Torchia, D. A. (1993) *Biochemistry*, 32, 6680–6687.

Baird, A., and Bohlen, R. (1990) In *Peptide Growth Factors and their Receptors* (Eds., Sporn, M., and Sporn, R.) Springer, New York, NY, pp. 369–418.

Basilico, C., and Moscatelli, D. (1992) *Adv. Cancer Res.*, 59, 115–165.

Bax, A., Clore, G. M., Driscoll, P. C., Gronenborn, A. M., Ikura, M. and Kay, L. E. (1990) *J Magn. Reson.*, 87, 620–627.

Bax, A., and Pochapsky, S. S. (1992) *J. Magn. Reson.*, 99, 638–643.

Carr, M. D., Birdsall, B., Frenkiel, T. A., Bauer, C. J., Jimenez-Barbero, J., Polshakov, V. I., McCormick, J. E., Roberts, G. C. K., and Feeney, J. (1991) *Biochemistry*, 30, 6330–6341.

Clore, G. M., and Gronenborn, A. M. (1989) *Crit. Rev. Biochem. Mol. Biol.*, 24, 479–564.

Clore, G. M., and Gronenborn, A. M. (1991a) *J. Mol. Biol.*, 221, 47–53.

Clore, G. M., and Gronenborn, A. M. (1991b) *Prog. NMR Spectrosc.*, 23, 43–92.

Clore, G. M., Wingfield, R. T., and Gronenborn, A. M. (1991) *Biochemistry*, 30, 2315–2323.

Delaglio, E., Grzesiek, S., Vuister, G. W., Zhu, G., Pfeifer, J., and Bax, A. (1995) *J. Biomol. NMR*, 6, 277–293.

Eriksson, A. E., Cousens, L. S., Weaver, L. H., and Matthews, B. W. (1991) *Proc. Natl. Acad. Sci. USA*, 88, 3441–3445.

Folkman, J., and Klagsbrun, M. (1987) *Science*, 235, 442–447.

Friedrichs, M. S., Mueller, L., and Wittekind, M. (1994) *J. Biomol. NMR*, 4, 703–726.

Garrett, D. S., Powers, R., Gronenborn, A. M., and Clore, G. M. (1991) *J Magn. Reson.*, 95, 214–220.

Gospodarowicz, D., and Cheng, J. (1986) *J Cell. Physiol.*, 128, 475–484.

Grzesiek, S., and Bax, A. (1992a) *J. Magn. Reson.*, 99, 201–207.

Grzesiek, S., and Bax, A. (1992b) *J. Magn. Reson.*, 96, 432–440.

Grzesiek, S., Anglister, J., and Bax, A. (1993) *J. Magn. Reson. Ser. B*, 101, 114–119.

Grzesiek, S., and Bax, A. (1993) *J. Biomol. NMR*, 3, 185–204.

Ikura, M., Kay, L. E., and Bax, A. (1991) *J. Biomol. NMR*, 1, 299–304.

Kabsch, W., and Sander, L. (1983) *Biopolymers*, 22, 2577–2637.

Kay, L. E., Ikura, M., Tschudin, R., and Bax, A. (1990) *J. Magn. Reson.*, 89, 496–514.

Li, L. Y., Safran, M., Aviezer, D., Boehlen, P., Seddon, A. P., and Yayon, A. (1994) *Biochemistry*, 33, 10999–11007.

Margalit, H., Fischer, N., and Ben-Sasson, S. A. (1993) *J Biol. Chem.*, 268, 19228–19231.

Marion, D., Ikura, M., Tschudin, R., and Bax, A. (1989a) *J. Magn. Reson.*, 85, 393–399.

Marion, D., Driscoll, P. C., Kay, L. E., Wingfield, P. T., Bax, A., Gronenborn, A. M. and Clore, G. M. (1989b) *Biochemistry*, 28, 6150–6156.

Marion, D., Kay, L. E., Sparks, S. W., Torchia, D. A., and Bax, A. (1989c) *J. Am. Chem. Soc.*, 111, 1515–1517.

Miyamoto, M., Naruo, K.-I., Seko, C., Matsumoto, S., Kondo, T., and Kurokawa, T. (1993) *Mol. Cell. Biol.*, 13, 4251–4259.

Moy, F. J., Lowry, D. F., Matsumura, P., Dahlquist, F. W., Krywko, J. E., and Domaille, P. J. (1994) *Biochemistry*, 33, 10731–10742.

Pantoliano, M. W., Horlick, R. A., Springer, B. A., Van Dyk, D. E., Tobery, T., Wetmore, D. R., Lear, J.D., Nahapetian, A. T., Bradley, J. D., and Sisk, W. P. (1994) *Biochemistry*, 33, 10229–10248.

Pineda-Lucena, A., Nunez de Castro, I., Lozano, R. M., Munoz-Willery, I., and Zazo, M. (1994a) *Eur. J. Biochem.*, 222, 425–431.

Pineda-Lucena, A., Jimenez, M. A., Nieto, J. L., Santoro, J., Rico, M., and Gimenez, G. G. (1994b) *J. Mol. Biol.*, 242, 81–98.

Powers, R., Gronenborn, A. M., Clore, G. M., and Bax, A. (1991a) *J. Magn. Reson.*, 94, 209–213.

Powers, R., Clore, G. M., Bax, A., Garrett, D. S., Stahl, S. J., Wingfield, P. T., and Gronenborn, A. M. (1991b) *J. Mol. Biol.*, 221, 1081–1090.

Powers, R., Garrett, D. S., March, C. J., Frieden, E. A., Gronenborn, A. M., and Clore, G. M. (1992) *Biochemistry*, 31, 4334–4346.

Reiland, J., and Rapraeger, A. C. (1993) *J. Cell. Sci.*, 105, 1085–1093.

Roghani, M., and Moscatelli, D. (1992) *J Biol. Chem.*, 267, 22156–22162.

Saksela, O., Moscatelli, D., Sommer, A., and Rifkin, D. B. (1988) *J. Cell Biol.*, 107, 743–751.

Seavey, B. R., Farr, E. A., Westler, W. M., and Markley, J. L. (1991) *J. Biomol. NMR*, 1, 217–230.

Seddon, A. P., Decker, M., Muller, T., Armellino, D., Kovesdi, I., Gluzman, Y., and Böhlen, P. (1991) *Ann. New York Acad. Sci.*, 638, 98–108.

Shirakawa, M., Fairbrother, W. J., Serikawa, Y., Ohkubo, T., Kyogoku, Y., and Wright, P. E. (1993) *Biochemistry*, 32, 2144–2153.

Sklenář, V., Piotto, M., Leppik, R., and Saudek, V. (1993) *J. Magn. Reson. Ser. A*, 102, 241–245.

Sommer, A., and Rifkin, D. B. (1989) *J Cell. Physiol.*, 138, 215–220.

Soteriou, A., Carr, M. D., Frenkiel, T. A., McCormick, J. E., Bauer, C. J., Sali, D., Birdsall, B., and Feeney, J. (1993) *J. Biomol. NMR*, 3, 535–546.

Spera, S., and Bax, A. (1991) *J. Am. Chem. Soc.*, 113, 5490–5492.

Thompson, L. D., Pantoliano, M. W., and Springer, B. A. (1994) *Biochemistry*, 33, 3831–3840.

Vuister, G. W., and Bax, A. (1993) *J. Am. Chem. Soc.*, 115, 7772–7777.

Westall, F.C., Rubin, R., and Gospodarowicz, D. (1983) *Life Sci.*, 33, 2425–2429.

Yayon, A., Klagsbrun, M., Esko, J. D., Leder, P., and Ornitz, D. M. (1991) *Cell*, 64, 841–848.

Zhang, J., Cousens, L. S., Barr, P. J., and Sprang, S. R. (1991) *Proc. Natl. Acad. Sci. USA*, 88, 3446–3450.

Zhu, X., Komiya, H., Chirino, A., Faham, S., Fox, G. M., Arakawa, T., Hsu, B. T., and Rees, D. C. (1983) *Science*, 251, 90–93.